# Shallow Si donor in ion-implanted homoepitaxial AIN

Cite as: Appl. Phys. Lett. **116**, 172103 (2020); https://doi.org/10.1063/1.5144080 Submitted: 03 January 2020 . Accepted: 08 April 2020 . Published Online: 27 April 2020

D M. Hayden Breckenridge, D Qiang Guo, Andrew Klump, D Biplab Sarkar, Yan Guan, James Tweedie, Ronny Kirste, Seiji Mita, D Pramod Reddy, Ramón Collazo, and D Zlatko Sitar







## **ARTICLES YOU MAY BE INTERESTED IN**

The nature of the DX state in Ge-doped AlGaN

Applied Physics Letters 116, 222102 (2020); https://doi.org/10.1063/5.0008362

The role of chemical potential in compensation control in Si:AlGaN Journal of Applied Physics 127, 105702 (2020); https://doi.org/10.1063/1.5132953

Molecular beam homoepitaxy on bulk AIN enabled by aluminum-assisted surface cleaning Applied Physics Letters 116, 172106 (2020); https://doi.org/10.1063/1.5143968





# Shallow Si donor in ion-implanted homoepitaxial AIN

Cite as: Appl. Phys. Lett. **116**, 172103 (2020); doi: 10.1063/1.5144080 Submitted: 3 January 2020 · Accepted: 8 April 2020 · Published Online: 27 April 2020







M. Hayden Breckenridge,<sup>1,a)</sup> D Qiang Guo,<sup>1</sup> Andrew Klump,<sup>1</sup> Biplab Sarkar,<sup>1</sup> Yan Guan,<sup>1</sup> James Tweedie,<sup>2</sup> Ronny Kirste,<sup>2</sup> Seiji Mita,<sup>2</sup> Pramod Reddy,<sup>2</sup> D Ramón Collazo,<sup>1</sup> and Zlatko Sitar<sup>1</sup> D

#### **AFFILIATIONS**

<sup>1</sup>Department of Material Science and Engineering, North Carolina State University, Raleigh, North Carolina 27695, USA <sup>2</sup>Adroit Materials, 2054 Kildaire Farm Road, Cary, North Carolina 27518, USA

#### **ABSTRACT**

We demonstrate Si as a shallow donor in aluminum nitride (AlN) with an ionization energy of  $\sim$ 70 meV. The shallow state was achieved by ion implantation of Si into homoepitaxial AlN and a low thermal budget damage recovery and activation process. These results demonstrate that the *DX* formation may be a kinetically limited process, though being a non-equilibrium process, preventing the Si donor from relaxing to the deep donor state. The room temperature conductivity was measured to be  $\sim$ 0.05  $\Omega^{-1}$  cm<sup>-1</sup>, which is one order of magnitude higher than what has been reported for the epitaxially doped or implanted AlN.

Published under license by AIP Publishing. https://doi.org/10.1063/1.5144080

Aluminum nitride (AlN) provides an attractive opportunity for the development of short wavelength (UVC) optoelectronic and next generation power electronic devices due to its ultra-wide bandgap of 6.1 eV, Schottky barriers >2 eV, and large breakdown field of 15 MV cm<sup>-1</sup>. In order to achieve highly conducting regions for optoelectronics and low doped drift regions for power electronics, the doping and compensation must be controlled over several orders of magnitude. n-type AlN has typically been attempted by introducing Si donor atoms during epitaxial growth. However, the achievable free electron concentration in Si-doped homoepitaxial AlN is currently limited to concentrations of  $\sim\!\!10^{15}\,\text{cm}^{-3}$  at room temperature.  $^{7-11}$  AlN films are typically grown on foreign substrates (e.g., sapphire) with dislocation densities (DD) >10<sup>9</sup> cm<sup>-2</sup>. 12-15 In contrast, AlN films grown by metal organic chemical vapor deposition (MOCVD) on AlN single crystal substrates have been shown to have DD <103 cm<sup>-2</sup>, making the DD-related compensation negligible. 16 Self-compensation by vacancy-Si complexes<sup>11,17</sup> and high concentrations of carbon (C<sub>N</sub>) have been observed also in homoepitaxially grown AlN films. 11 In addition, the low free carrier concentration relative to the doping concentration has been attributed to the formation of a presumed Si DX center associated with off-site relaxation of Si<sub>Al</sub> that compensates the free electrons. 7,9,18,19 This self-compensation results in the "pinning" of the bulk Fermi level and a significantly higher ionization energy ( $E_i \sim 250-320 \,\mathrm{meV}$ ) than that predicted by the

hydrogenic model ( $\sim$ 75 meV) and, hence, it is deemed responsible for limiting the achievable free carrier concentration.  $^{7,9,20,21}$ 

Theoretical work (density functional theory) has predicted a large lattice relaxation for Si in AlN, resulting in a DX center represented by a -1/+1 transition at  $\sim 200$  meV. <sup>19</sup> Interestingly, photoluminescence studies have shown the presence of a shallow Si donor  $(d^{0/+})$  in addition to the deep center (DX<sup>-</sup>). <sup>22,23</sup> Furthermore, the work by Zeisel et al. concluded that there should be an energy barrier between the shallow donor state,  $d^{0/+}$ , and the deep acceptor state,  $DX^-$ , which should determine the population of each state according to the equilibrium conditions. Furthermore, since the incorporation of species during growth is dominated by surface diffusion, and energy barriers at the surface are significantly lower than in the bulk, the concentration of Si atoms that relax into the DX<sup>-</sup> state should be high during epitaxy. However, in the case of a non-equilibrium process, such as ion implantation, DX formation essentially occurs in the bulk and may be kinetically inhibited and the occupancy distribution of each state may deviate from the expected equilibrium distribution. Hence, doping via ion implantation at low temperatures may significantly reduce the concentration of Si atoms that relax into the DX acceptor state, ultimately allowing for realization of lower compensation and higher free carrier concentrations.

In general, ion implantation is a basic semiconductor technology used for the lateral control of doping and fabrication of planar electronic devices and integrated circuits. Its use is fundamental for power

a) Author to whom correspondence should be addressed: mhbrecke@ncsu.edu

devices and, as such, its development is a part of the essential technological toolbox for any semiconductor technology. In this work, we investigate the hypothesis that a non-equilibrium process, such as Si implantation, can be implemented to inhibit the formation of the  $DX^-$  state, providing for higher free carrier concentrations.

The challenge associated with ion implantation into the ultrawide bandgap materials is the creation of point defects (lattice damage) that can lead to self-compensation  $^{24}$  and a negative impact on both the electrical and optical properties of the material. High temperature annealing is necessary to repair the lattice damage and activate the dopant atoms. Kanechika and Kachi have demonstrated the ability to recover a significant portion of the implantation damage in AlN films grown on sapphire by annealing at  $1400\,^{\circ}\mathrm{C}.^{24}$  However, the observed donor activation energy was characteristic of the  $DX^-$  state and the free electron concentrations measured by Hall were similar to those of the epitaxially doped AlN, indicating that a similar equilibrium condition as during growth had been reached. In order to test the above hypothesis, this work aims to achieve doping at lower damage levels and lower thermal budgets where the system does not reach an equilibrium.

For this work, AlN homoepitaxial films were grown via metal organic chemical vapor deposition (MOCVD) on single crystal AlN substrates  $^{25-27}$  at a temperature of  $1100\,^{\circ}\mathrm{C}$  and a total pressure of 20 Torr. The V/III ratio of 1000 was established by flowing 8.4  $\mu$ mol/min of trimethylaluminum (TMA) and 0.3 slm of ammonia at a total flow rate of 10 slm with the hydrogen diluent. Further details pertaining to AlN homoepitaxial growth are described elsewhere.  $^{16,28,29}$  Si was implanted into the homoepitaxial AlN films at room temperature with a dose of  $1\times10^{14}$  atoms/cm $^2$  and an acceleration voltage of 100 keV. A tilt angle of  $7^{\circ}$  was used to reduce ion channeling during implantation.

The implanted AIN films were characterized with secondary ion mass spectrometry (SIMS) to determine the depth profile of the implanted Si ions and background impurity concentration. The optical properties of the AlN films were characterized by photoluminescence spectroscopy (PL) at a temperature of 3 K using a 193 nm ArF excimer laser with a pulse width of 5 ns and a repetition rate of 100 Hz and a power density of ∼5 kW/cm<sup>2</sup>. Optical spectra were collected with a Princeton Instruments Acton SP2750 0.75 m high-resolution spectrograph with a 3200 grooves/mm optical grating and a PIXIS: 2KBUV Peltier-cooled charge-coupled device camera, allowing for a spectra resolution of  $\sim$ 50  $\mu$ eV. This high spectra resolution is suitable to record the sharp band edge emission associated with the high crystalline quality AlN homoepitaxy. The crystal quality and lattice damage of each sample were assessed with the use of high-resolution x-ray diffraction (HR-XRD) following growth, ion implantation, and high temperature annealing. HR-XRD scans were recorded using a Philips X'Pert Materials Research Diffractometer system. The Cu K<sub>∞</sub> x-rays were conditioned in point focus with a four-bounce Ge [220] monochromator. ω-rocking curves were recorded on-axis in an open detector geometry. Two post-implantation annealing temperatures were implemented in this work. One sample was annealed at 1200 °C, while another was annealed at 1500 °C. Both annealing processes were performed for 120 min in a nitrogen atmosphere and at a pressure of 100 Torr. For the electrical studies, approximately 80 nm of AlN was reactive ion etched using BCl<sub>3</sub>/Cl<sub>2</sub> chemistry in a Trion Technology Minilock II to access peak Si concentration. V/Al/Ni/Au (30/100/70/ 70 nm) contacts in the van der Pauw geometry were deposited onto the etched surface by electron beam evaporation. Contacts were annealed via rapid thermal annealing at 850 °C for 60 s. The carrier type, concentration, and mobility at higher temperatures were determined using a 8400 series LakeShore AC/DC Hall measurement system. Temperature dependent resistivity measurements were obtained using a four-point probe setup in a temperature range of 300–750 K.

The as-implanted Si SIMS depth profile is shown in Fig. 1. The maximum Si concentration of approximately  $9 \times 10^{18} \, \mathrm{cm}^{-3}$  with a range of approximately 120 nm and a straggle of  $\sim 50 \, \mathrm{nm}$  was obtained. Higher than expected Si concentrations ( $\sim 1 \times 10^{17} \, \mathrm{cm}^{-3}$ ) were observed past 600 nm in the c-direction, which may be due to some channeling.

Prior to implantation,  $\omega$ -rocking curves were measured to evaluate the crystallinity of the AlN films grown homoepitaxially via MOCVD. 30,31 Rocking curve full-width half maximum (FWHM) values of the (0 0.2) reflection were 12-18 arc sec for all the as-grown samples.<sup>32</sup> Using symmetric  $\omega$ -2 $\theta$  scans, the progression from the as-grown to damaged AlN film due to the implantation damage is readily observed. 32,33 The damage is characterized by the appearance of an additional strain-related peak at lower angles, which appears as additional diffracted intensity at low Qz in the reciprocal space map (RSM) of the symmetric (0 0.2) reflection [Fig. 2(a)]. Since the implantation-induced lattice disorder has a negative influence upon the electrical and optical properties of the implanted layer,<sup>36</sup> an annealing process is crucial to remove lattice disorder and electrically activate the Si ions by thermally stimulating their transition to energetically favorable lattice sites.<sup>37</sup> XRD characterization of the implanted homoepitaxial AlN films after annealing at 1200 °C for 120 min showed practically full recovery of the crystal lattice [Fig. 2(b)], as signified by the disappearance of the strain-related intensity at low Q<sub>z</sub>. An RSM of the asymmetric (1 0 3) reflection (Fig. 3) showed that the lattice damage was confined primarily to Q<sub>2</sub>, indicative of the damage occurring in the direction parallel to the implantation. Thus, the main impact on the crystallography of the film after ion implantation is the c-lattice expansion. However, more detailed studies are required to evaluate structural characteristics of the implantation and annealing processes in detail.

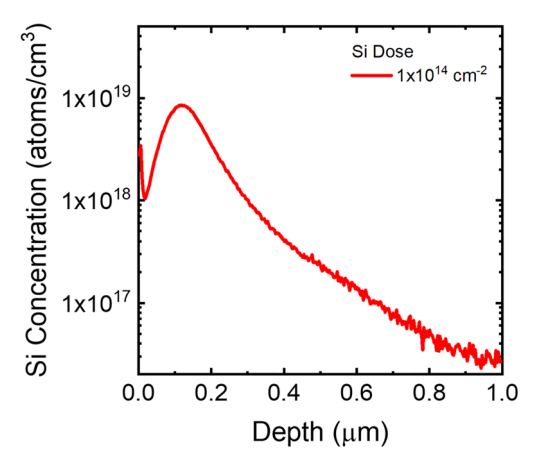


**FIG. 1.** SIMS data showing the room temperature Si implantation profile for a Si dose of  $1\times10^{14}\,\mathrm{cm}^{-2}$  and an ion energy of 100 keV.

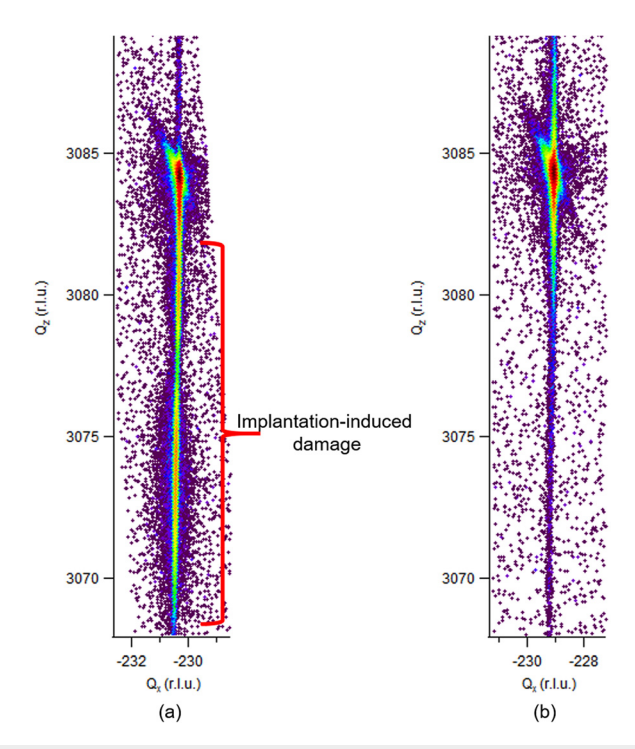


**FIG. 2.** (0 0.2) reciprocal space maps of the AIN homoepitaxial film (a) as implanted and (b) after annealing for 120 min at 1200  $^{\circ}$ C in N<sub>2</sub>.

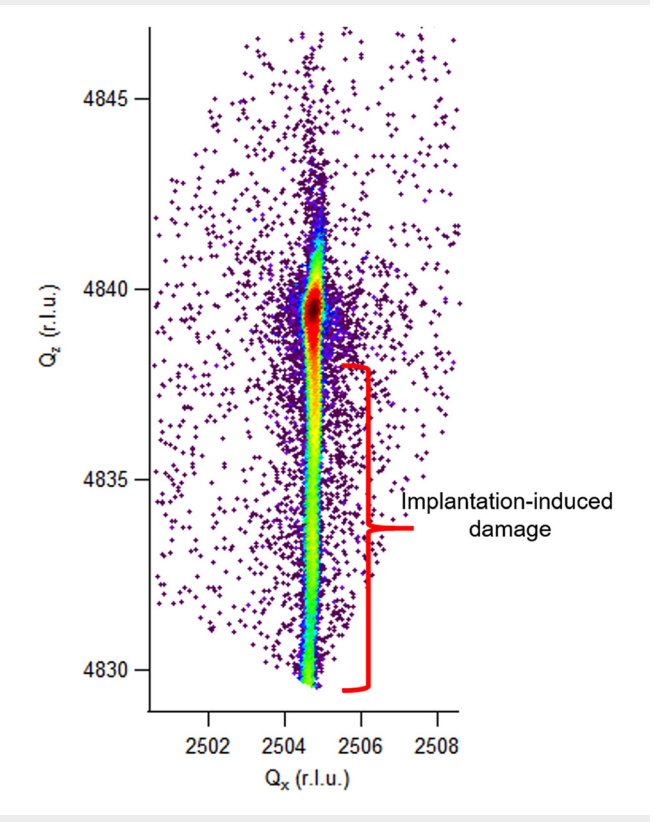
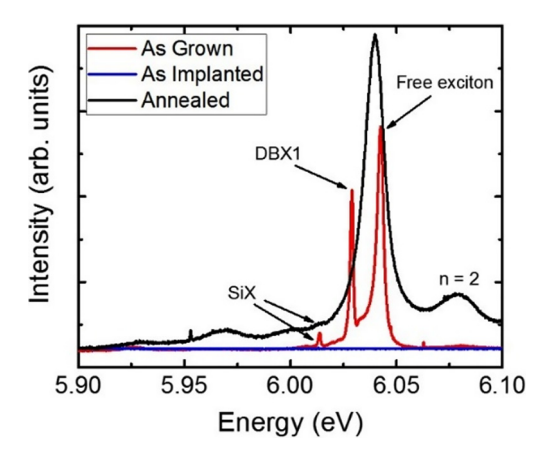


FIG. 3. (1 0.3) reciprocal space map of the AIN homoepitaxial film as implanted.

The implantation-induced damage and the subsequent recovery of the AlN lattice were also characterized with PL. The as-grown AlN films (Fig. 4, red curve) demonstrated free and donor bound exciton emissions with narrow FWHMs of approximately 500  $\mu$ eV, indicative of excellent crystalline quality. No defect-related mid gap luminescence was observed for the as-grown samples. In contrast, the as-implanted samples showed no luminescence (Fig. 4, blue curve), confirming the presence of copious implantation-induced non-radiative point defects. Following the annealing process, a recovery of the excitonic emission (Fig. 4, black curve) was observed, indicative of the restoration of the crystalline order. The excitonic emission was broadened to a FWHM of approximately 2 meV. Some broadening was expected due to the relatively high Si concentration; however, at this point it is not clear if any possible remnant lattice disorder contributed to this broadening as well.

Following the annealing, electrical studies were performed. Both the hot probe test at room temperature and the AC Hall effect measurement performed at  $400\,^{\circ}\mathrm{C}$  confirmed that the annealed and Si implanted samples were both n-type. Despite observing higher margins of error associated with the AC Hall at lower temperatures, four-point-probe measurements confirmed that the samples were electrically conductive at room temperature. In contrast, the as-grown, unintentionally doped AlN films and as-implanted samples were electrically insulating. The reported conductivity and free carrier concentrations were calculated using a Si doping thickness of  $200\,\mathrm{nm}$  (estimated using the SIMS data from Fig. 1).

Figure 5 compares the conductivity as a function of temperature for the epitaxially Si doped AlN (black triangles), previous reports of Si implanted AlN films grown on sapphire (green squares),  $^{24}$  and the two Si implanted homoepitaxially grown AlN samples from this work annealed at 1200 °C (red squares) and 1500 °C (blue squares) for 120 min. The room temperature electrical conductivity of  $\sim\!0.05~\Omega^{-1}$  cm $^{-1}$  was measured for our implanted sample that was annealed at 1200 °C, which is approximately one order of magnitude higher than that of our epitaxially doped AlN, the Si implanted sample annealed at 1500 °C, and the literature reports on Si implantation. Using the AC



**FIG. 4.** Damage and recovery of the AIN crystal lattice as shown by the near band edge photoluminescence spectra measured at  $T=3\,\mathrm{K}$ . The spectra were shifted vertically for better visibility. As grown AIN (red), after implantation (blue), and after annealing at 1200 °C for 120 min (black).

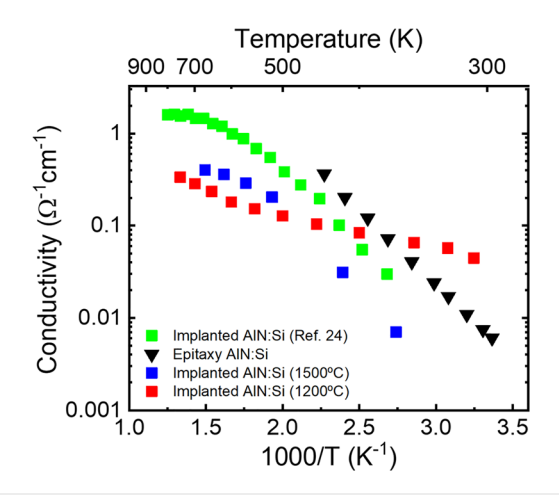


**FIG. 5.** Conductivity as a function of temperature for the epitaxially doped AlN (black triangles), previous reports of Si implanted AlN films grown on sapphire (green squares),  $^{24}$  and implanted samples from this work either annealed at 1500 °C (blue squares) or 1200 °C (red triangles).

Hall effect at 400 °C, we can report the free electron concentrations and mobilities for both Si implanted samples annealed for 120 min at either 1200 °C or 1500 °C. For the sample annealed at 1200 °C, the free electron concentration is  $\sim\!\!2\times10^{18}\,\rm cm^{-3}$  and an electron mobility of  $\sim\!\!1\,\rm cm^2/V\,s$ , whereas the sample annealed at 1500 °C, was measured to have a free carrier concentration of  $\sim\!\!8\times10^{16}\,\rm cm^{-3}$  and a mobility of  $\sim\!\!32\,\rm cm^2/V\,s$ . Interestingly, the free carrier concentration for the lower temperature annealing condition (1200 °C) is more than an order of magnitude higher than that of the Si implanted sample annealed at 1500 °C and is attributed to DX inhibition and consequently low activation energy as will be discussed in the following.

From the temperature dependent conductivity measurements, we estimated the donor ionization energy  $(E_i)$  for all samples using <sup>38,39</sup>

$$\sigma = \sigma_0 T^{-2} e^{\frac{-E_i}{k_B T}}.\tag{1}$$

The epitaxially doped AlN sample and the Si implanted AlN sample annealed at 1500 °C had Si ionization energies of  $\sim$ 250 meV, in agreement with previous reports, <sup>7,9</sup> while our implanted and annealed (1200 °C) AlN samples exhibited a significantly lower ionization energy,  $E_i \sim$ 70 meV, which is in good agreement with the predicted ionization energy using the hydrogenic model for a shallow donor in AlN given by

$$E_i = \frac{m_e^* e^4}{2(4\pi\varepsilon\hbar)^2} = \frac{m_e}{m_e^* \varepsilon^2} E_H \approx 75 \text{ meV}, \tag{2}$$

with  $\varepsilon=8.5$ ,  $m_e^*/m_e=0.4$ . The higher conductivity and lower impurity ionization energy in the implanted sample using a lower annealing temperature (1200 °C) suggest that a majority of the Si atoms were at the shallow donor state and not in the relaxed deep acceptor  $DX^-$  state. By comparison, the implanted AlN:Si with damage recovery annealing at 1400 °C (Ref. 24) had  $E_i \sim$ 290 meV, comparable to the ionization energy reported for the epitaxially doped AlN. As shown in Fig. 5, the slope for the sample annealed at 1500 °C is similar to the slopes for the epitaxially doped sample and the work from Kanechika

and Kachi,<sup>24</sup> indicating that the DX related compensation is present. These results suggest that the annealing of highly disordered AlN samples at high temperatures brought the system closer to the equilibrium and allowed it to relax into a DX-state, while the lower thermal budget produced a desired and predicted shallow donor state. This validates the hypothesis of kinetically inhibiting the formation of  $DX^-$  states by managing the kinetics of the annealing process.

Although the films annealed with a low thermal budget showed almost one order of magnitude higher conductivity at room temperature compared to the implantation work in Ref. 24, the implanted sample annealed at 1500  $^{\circ}$ C, and the epitaxially doped sample (Fig. 5), at temperatures >500 K, a lower conductivity was observed. This is indicative of significant compensation, other than the DX, in the implanted films.

In conclusion, Si implantation was realized in homoepitaxial AlN films. Based on HR-XRD and PL results, the implantation-induced damage was practically completely reduced already at  $1200\,^{\circ}\text{C}$ . Electrical measurements showed an order of magnitude higher n-type conductivity ( $\sim\!0.05~\Omega^{-1}~\text{cm}^{-1}$ ) at room temperature in Si implanted AlN films as compared to epitaxially doped ones, with an estimated carrier concentration  $>\!1\times10^{17}~\text{cm}^{-3}$  at room temperature. The ionization energy for the Si donor was estimated to be  $\sim\!70~\text{meV}$ , which is similar to the ionization energy predicted by the hydrogenic model. These results suggest that ion implantation, as a non-equilibrium process, may provide an avenue to manage the population distribution between the two possible Si states in AlN, a shallow donor and a deep acceptor state, and at the same time provide an avenue for selective n-type doping in AlN.

The authors acknowledge funding in part from the NSF (Nos. ECCS-1508854, ECCS-1610992, DMR-1508191, and ECCS-1653383), ARO (Nos. W911NF-15-2-0068 and W911NF-16-C-0101), and AFOSR (No. FA9550-17-1-0225).

### **REFERENCES**

<sup>1</sup>H. Angerer, D. Brunner, F. Freudenberg, O. Ambacher, M. Stutzmann, R. Höpler, T. Metzger, E. Born, G. Dollinger, A. Bergmaier, S. Karsch, and H.-J. Körner, Appl. Phys. Lett. **71**, 1504 (1997).

<sup>2</sup>Q. Guo and A. Yoshida, Jpn. J. Appl. Phys., Part 1 33, 2453 (1994).

<sup>3</sup>T. Kinoshita, T. Nagashima, T. Obata, S. Takashima, R. Yamamoto, R. Togashi, Y. Kumagai, R. Schlesser, R. Collazo, A. Koukitu, and Z. Sitar, Appl. Phys. Express 8, 061003 (2015).

<sup>4</sup>P. Reddy, I. Bryan, Z. Bryan, J. Tweedie, R. Kirste, R. Collazo, and Z. Sitar, J. Appl. Phys. **116**, 194503 (2014).

5J. Xie, S. Mia, R. Dalmau, R. Collazo, A. Rice, J. Tweedie, and Z. Sitar, Phys. Status Solidi C 8, 2407 (2011).

<sup>6</sup>J. Y. Tsao, S. Chowdhury, M. A. Hollis, D. Jena, N. M. Johnson, K. A. Jones, R. J. Kaplar, S. Rajan, C. G. V. de Walle, E. Bellotti, C. L. Chua, R. Collazo, M. E. Coltrin, J. A. Cooper, K. R. Evans, S. Graham, T. A. Grotjohn, E. R. Heller, M. Higashiwaki, M. S. Islam, P. W. Juodawlkis, M. A. Khan, A. D. Koehler, J. H. Leach, U. K. Mishra, R. J. Nemanich, R. C. N. Pilawa-Podgurski, J. B. Shealy, Z. Sitar, M. J. Tadjer, A. F. Witulski, M. Wraback, and J. A. Simmons, Adv. Electron. Mater. 4, 1600501 (2018).

<sup>7</sup>R. Zeisel, M. W. Bayerl, S. T. B. Goennenwein, R. Dimitrov, O. Ambacher, M. S. Brandt, and M. Stutzmann, Phys. Rev. B 61, R16283 (2000).

<sup>8</sup>Y. Taniyasu, M. Kasu, and T. Makimoto, Appl. Phys. Lett. **85**, 4672 (2004).

<sup>9</sup>R. Collazo, S. Mita, J. Xie, A. Rice, J. Tweedie, R. Dalmau, and Z. Sitar, Phys. Status Solidi C 8, 2031 (2011).

<sup>10</sup>E. C. H. Kyle, S. W. Kaun, P. G. Burke, F. Wu, Y.-R. Wu, and J. S. Speck, J. Appl. Phys. 115, 193702 (2014).

- <sup>11</sup>I. Bryan, Z. Bryan, S. Washiyama, P. Reddy, B. Gaddy, B. Sarkar, M. H. Breckenridge, Q. Guo, M. Bobea, J. Tweedie, S. Mita, D. Irving, R. Collazo, and Z. Sitar, Appl. Phys. Lett. 112, 062102 (2018).
- <sup>12</sup>K. Nakano, M. Imura, G. Narita, T. Kitano, Y. Hirose, N. Fujimoto, N. Okada, T. Kawashima, K. Iida, K. Balakrishnan, M. Tsuda, M. Iwaya, S. Kamiyama, H. Amano, and I. Akasaki, Phys. Status Solidi A 203, 1632 (2006).
- <sup>13</sup>H. Hirayama, S. Fujikawa, N. Noguchi, J. Norimatsu, T. Takano, K. Tsubaki, and N. Kamata, Phys. Status Solidi A 206, 1176 (2009).
- <sup>14</sup>J. Bai, M. Dudley, W. H. Sun, H. M. Wang, and M. A. Khan, Appl. Phys. Lett. 88, 051903 (2006).
- <sup>15</sup>H. Miyake, G. Nishio, S. Suzuki, K. Hiramatsu, H. Fukuyama, J. Kaur, and N. Kuwano, Appl. Phys. Express 9, 025501 (2016).
- <sup>16</sup>R. Dalmau, B. Moody, R. Schlesser, S. Mita, J. Xie, M. Feneberg, B. Neuschl, K. Thonke, R. Collazo, A. Rice, J. Tweedie, and Z. Sitar, J. Electrochem. Soc. 158, H530 (2011)
- <sup>17</sup>S. F. Chichibu, H. Miyake, Y. Ishikawa, M. Tashiro, T. Ohtomo, K. Furusawa, K. Hazu, K. Hiramatsu, and A. Uedono, J. Appl. Phys. 113, 213506 (2013).
- <sup>18</sup>M. Feneberg, B. Neuschl, K. Thonke, R. Collazo, A. Rice, Z. Sitar, R. Dalmau, J. Xie, S. Mita, and R. Goldhahn, Phys. Status Solidi A 208, 1520 (2011).
- <sup>19</sup>L. Gordon, J. L. Lyons, A. Janotti, and C. G. Van de Walle, Phys. Rev. B 89, 085204 (2014).
- N. T. Son, M. Bickermann, and E. Janzén, Phys. Status Solidi C 8, 2167 (2011).
  B. Borisov, V. Kuryatkov, Yu. Kudryavtsev, R. Asomoza, S. Nikishin, D. Y. Song, M. Holtz, and H. Temkin, Appl. Phys. Lett. 87, 132106 (2005).
- 22 B. Neuschl, K. Thonke, M. Feneberg, S. Mita, J. Xie, R. Dalmau, R. Collazo, and Z. Sitar, Phys. Status Solidi B 249, 511 (2012).
- 23B. Neuschl, K. Thonke, M. Feneberg, R. Goldhahn, T. Wunderer, Z. Yang, N. M. Johnson, J. Xie, S. Mita, A. Rice, R. Collazo, and Z. Sitar, Appl. Phys. Lett. 103, 122105 (2013).

- <sup>24</sup>M. Kanechika and T. Kachi, Appl. Phys. Lett. **88**, 202106 (2006).
- 25Z. G. Herro, D. Zhuang, R. Schlesser, R. Collazo, and Z. Sitar, J. Cryst. Growth 286, 205 (2006).
- <sup>26</sup>D. Zhuang, Z. G. Herro, R. Schlesser, and Z. Sitar, J. Cryst. Growth 287, 372 (2006).
- <sup>27</sup>P. Lu, R. Collazo, R. F. Dalmau, G. Durkaya, N. Dietz, B. Raghothamachar, M. Dudley, and Z. Sitar, J. Cryst. Growth 312, 58 (2009).
- <sup>28</sup>I. Bryan, A. Rice, L. Hussey, Z. Bryan, M. Bobea, S. Mita, J. Xie, R. Kirste, R. Collazo, and Z. Sitar, Appl. Phys. Lett. 102, 061602 (2013).
- <sup>29</sup> A. Rice, R. Collazo, J. Tweedie, R. Dalmau, S. Mita, J. Xie, and Z. Sitar, J. Appl. Phys. **108**, 043510 (2010).
- 30 M. A. Moram and M. E. Vickers, Rep. Prog. Phys. 72, 036502 (2009).
- <sup>31</sup>J. E. Ayers, J. Cryst. Growth **135**, 71 (1994).
- <sup>32</sup>W. Guo, J. Xie, C. Akouala, S. Mita, A. Rice, J. Tweedie, I. Bryan, R. Collazo, and Z. Sitar, J. Cryst. Growth 366, 20 (2013).
- 33S. Hayashi, B. Poust, B. Heying, and M. Goorsky, in 2003 International Symposium on Compound and Semiconductors (IEEE, 2003), pp. 106–107.
- 34 U. Dadwal, R. Scholz, P. Kumar, D. Kanjilal, S. Christiansen, U. Gösele, and R. Singh, Phys. Status Solidi A 207, 29 (2010).
- 35C. Ventosa-Moulet, S. Hayashi, and M. S. Goorsky, ECS Trans. 33, 249 (2010).
- 36 J. F. Ziegler, Ion Implantation Science and Technology (Elsevier, 2012).
- <sup>37</sup>S. O. Kucheyev, J. S. Williams, and S. J. Pearton, Mater. Sci. Eng. R 33, 51 (2001).
- <sup>38</sup>S. M. Sze and K. K. Ng. *Physics of Semiconductor Devices*, 3rd ed. (Wiley-Interscience, Hoboken, NJ, 2006).
- <sup>39</sup>T. T. Mnatsakanov, M. E. Levinshtein, L. I. Pomortseva, S. N. Yurkov, G. S. Simin, and M. Asif Khan, Solid-State Electron. 47, 111 (2003).
- <sup>40</sup>K. Zhu, M. L. Nakarmi, K. H. Kim, J. Y. Lin, and H. X. Jiang, Appl. Phys. Lett. 85, 4669 (2004).